Nanotwin assisted reversible formation of low angle grain boundary upon reciprocating shear load

Shuang Li[a,#], Nanjun Chen[b,#], Aashish Rohatgi[c], Yulan Li[b], Cynthia A. Powell[c], Suveen Mathaudhu[c,d], Arun Devaraj[b], Shenyang Hu[e*], Chongmin Wang[a*]

[a]Environmental Molecular Sciences Laboratory, Pacific Northwest National Laboratory, Richland, WA 99352, USA
[b]Physical and Computational Sciences Directorate, Pacific Northwest National Laboratory, Richland, WA99352, USA
[c]Energy and Environment Directorate, Pacific Northwest National Laboratory, Richland, WA99352, USA
[d]Metallurgical and Materials Engineering Department, Colorado School of Mines, Golden, CO 80401, USA
[e]National Security Directorate, Pacific Northwest National Laboratory, Richland, WA 99352

[#] S.L. and N.C. contributed equally to this work.
[*]Corresponding authors: shenyang.hu@pnnl.gov, chongmin.wang@pnnl.gov

Keywords: *in-situ* TEM, grain boundary formation, shear deformation, twin

Abstract:

Severe plastic deformation of metals is known to lead to superior properties that cannot be achieved by any traditional metallurgic process. Origin of the superior properties is perceived to be closely associated with grain refinement, a fundamental process during the severe plastic deformation, which is essentially the formation of new grain boundaries. However, the atomistic mechanism of grain boundary formation remains largely obscure. Here, by using *in-situ* transmission electron microscopy and molecular dynamic simulation, we reveal, for the first time at atomic level, shear-induced low-angle grain boundary (LAGB) formation processes in Au nanocrystal. We discover the LAGB formation is accomplished through inward propagation of nanotwins accompanied by dislocations gliding on twin boundaries, a nanotwin-mediated dislocation slip mechanism, which shows reversible characteristic under reciprocating shear load and is affected by the nanocrystal microstructure and orientation. Our result unveils unprecedented atomistic insights on shear driven grain refinement towards nanostructure of superior properties.

1. Introduction

Severe plastic deformation (SPD) of metallic materials has been well realized to lead to a wealth of unique mechanical properties[1, 2], such as ultrahigh strength, high elasticity, and superplasticity. The superior mechanical property is perceived to be closely associated with grain refinement of the materials, featuring the formation of a nanostructure that is populated with high density of grain boundaries, and correspondingly leading to the unique deformation mechanisms[3-5] with superior properties. Typically, for the face centered cubic (fcc) metals, the dominant deformation mechanism translates from dislocation slip to twinning when the characteristic size of grain decreases to about several 10 nm[6, 7], contributing to super-ductility. With the grain size being refined to the scale of ~ 10 nm[8-10], the deformation is dominated by grain boundary sliding and grain rotation, attributing to the softening of the material.

Shear deformation, a dominant deformation mechanism of SPD[2, 11, 12], plays a significant role in producing ultrafine-grain and nanocrystalline microstructures with superior properties. Based on intensive *ex-situ* studies, several microstructural evolution processes have been proposed to account for the mechanically driven grain refinement, such as dislocation-mediated grain refinement[13, 14], interaction of twins and dislocations induced grain subdivision[15], GB migration controlled grain evolution[16], and dynamic recrystallization[17]. Lu et al. found that plastic strain induced grain refinement in Cu depends on the strain rate, evolving from dislocation cell walls dominated process at low strain rate to nanometer-thick twins dominated one at high strain rate[18], and leading to four possible mechanisms for the deformation twin/matrix lamellae induced grain refinement[19]. These studies clearly demonstrate the key roles of dislocations and twins in grain refinement. However, associated with the *ex-situ* analyses that relies on exclusively the snapshots of the initial and final state, the dynamic atomic process of GB formation under shear deformation is essentially far from clear.

Here, by combining *in-situ* TEM nanomechanical deformation and molecular dynamic simulation, we capture the atomistic processes of shear-induced low angle grain boundary (LAGB) formation in Au nanocrystal. We reveal, at atomic level, a nanotwin assisted LAGB formation dynamics, which is characteristically featured by a nanotwin-mediated dislocation slip mechanism and shows excellent reversibility with negligible damage accumulation under reciprocating shear load. The reversible deformation is governed by the cooperative propagation of nanotwin and full

dislocation, where the twin boundary (TB) acts as the slip plane for dislocation gliding. The LAGB formation mechanism is found to show dependence on the orientation of the nanocrystal and the pre-existing twin. This work reveals the dynamic mechanism of the reversible LAGB formation, offering unprecedented atomistic insights on shear driven microstructure evolution in metallic nanomaterials towards superior properties.

2. Materials and Methods

2.1. *In-situ* TEM nanofabrication and shear testing

Bulk Au rods with a diameter of 0.25 mm and a purity of 99.99 wt.% was ordered from Goodfellow. The bulk Au rods was cut by a wire cutter to obtain numerous single crystalline tips with nanoscale at the fracture surface, as shown in Supplementary Figure 1. Two Au rods after fracture were loaded on the two sides of the nanofactory TEM-scanning tunneling microscope (STM) holder where one side was movable and controlled by a piezo-manipulator. The properly selected nanotips with <110> zone axis in both sides were connected to fabricate Au nanocrystal inside TEM by cold welding with pre-applied voltage. Then *in-situ* reciprocating shear load was carried out on the as-fabricated nanocrystal at room temperature by moving the piezo-manipulator side leftward/rightward slowly with a constant speed about 0.5 nm s^{-1}. The *in-situ* nanofabrication and shear load were carried out inside a FEI Titan Cs-corrected TEM operated at 300 kV. All *in-situ* experiments were performed under weak beam conditions to minimize the potential beam effects on deformation and recorded in real time by a charge-coupled device (CCD) camera at a rate of 0.2 s per frame. For easily observe the phenomena, the Supplementary Movie 1 and 3 was played at 10 times speed and 2 times speed, respectively. The Supplementary Movie 5 was played at original capture speed.

2.2. Molecular dynamics simulations

Molecular dynamics (MD) simulations were carried out for studying the shear deformation on a gold single crystal. The model was designed in a way close to the experiment setup, shown in Supplementary Figure 2. The orientation of the crystal was set with [1-10] direction parallel to the y axis. Two slabs of rigid atoms with a thickness (z direction) of 1.4nm were fixed at the top and bottom of the material, respectively. The shear deformations were operated at 300K with a constant shear load applied at the bottom at a velocity of 1m/s. A schematic of the reciprocating shear load

was illustrated in Supplementary Figure 2c with shear distance showing in x direction. The Large-scale Atomic/Molecular, Massively Parallel Simulator (LAMMPS)[20] was used to perform the calculations. The velocity Verlet algorithm was employed to integrate the Newton's equations of motion with a timestep of 1fs. The atomic interaction was described by embedded atom method (EAM) potentials[21] for Au with a prediction of stacking fault energy (SFE) to be 42.59 mJ/m^2. This value has well reproduced the experimental estimation (52 ± 15 mJ/m^2) [22]. Ovito software was utilized for MD data visualization and analysis[23]. By using common neighbor analysis (CNA)[24], different local structures can be identified. The corresponding local structures, i.e. other (disordered atoms/dislocation cores), fcc, and hcp were indicated in white, green, and red, respectively, throughout the study unless specified. The lattice misorientation is calculated by polyhedral template matching modifier[25] implemented in Ovito, which provides the local lattice orientation for atoms that match one of the structural types. The rotation angle is estimated by referencing its initial lattice orientation.

3. Results

3.1. Reversible LAGB formation under reciprocating shear load

An Au nanocrystal with [1-10] zone axis was fabricated by the nano-weld method inside a transmission electron microscope (TEM) as detailed in the Methods. Figure 1a shows high resolution TEM (HRTEM) image of the as-fabricated Au nanocrystal with a geometry of 15 nm at the bottom and 30 nm at the top. The nanocrystal includes a pre-existing {111}<112> twin as indicated by the insert FFT pattern. The bottom of the Au nanocrystal connected with a piezo manipulator which could move horizontally to produce a shear deformation. The shear stress had an inclination of ~11° relative to the (111) plane of the Au nanocrystal as indicated by the white arrow in Figure 1b.

The LAGB formation and annihilation under reciprocating shear load are shown in Figure 1b-h and Supplementary Movie 1. Figure 1b shows the snapshot at 17 s under the rightward shear, featuring the alignment of the frontier of nanotwins from the free surface. Each nanotwin is accompanied by a dislocation with an excess (111) plane. These dislocations spontaneously align to form a LAGB with misorientation angle of $5°$. We notice that, instead of free surface,

dislocations also can nucleate on the pre-existing TB and within the pre-existing twin. The early deformation stage prior to Figure 1b is displayed in the Supplementary Figure 3. From the snapshot at 5s (Supplementary Figure 3a), a leading Shockley partial dislocation slid along the TB, resulting in the shrink of the pre-existing twin and a dislocation with an excess (111) plane at the end of the shrink segment. In the snapshot at 7s (Supplementary Figure 3b), two nanotwins marked 1 and 2 nucleated from the free surface. With the increase of shear deformation, the number of dislocations and nanotwins increases, which is accompanied by the upward migration of the LAGB and increased misorientation angle (Figure 1b-d), as measured from the HRTEM snapshot and the corresponding FFT pattern (Supplementary Figure 4). Annihilation of unstable nanotwins could be noticed, such as the one marked as '7'. The nanotwin appeared in the snapshot at 24 s, but disappeared at 39 s, then appeared again at 41 s. However, the number of the nanotwins increases with increased shear deformation. Besides the dislocations at the head of the nanotwins, dislocation also existed beside the nanotwin below the LAGB as representatively shown by '1'' and '4' nanotwins in Figure 1d, implying the nanotwin growth, dislocation nucleation and glide occur simultaneously. Nanotwins, as representatively marked as '1' and '4' in Figure 1c, d, could even transfer across the LAGB under severe shear deformation. The configuration of dislocations, nanotwins, and LAGB with respect to the shear load direction is schematically shown in Figure 1e.

Reversed shear deformation resulted in the backwards migration of LAGB with decreasing misorientation angle until the plastic deformation was mostly recovered, as shown in Figure 1f-h. Association of migrating dislocations with the detwinning of the deformation nanotwin further confirms the codependent relationship between nanotwin and dislocation. The deformation recover process has a hysteresis with some deformation energy stored in the nanocrystal. To illustrate the hysteresis, we draw the LAGB migration displacement, misorientation angle beside LAGB and dislocation number versus shear displacement of the nanocrystal at the bottom (Figure 1i). The LAGB migration displacement starts to decrease as soon as the load is reversed, whereas the decreases of the misorientation angle and the dislocation number appear delayed following the reversed load of 6 nm and 3 nm shear displacement in the reversed direction. The maximum shear strain during the reversible behavior is about 0.32, which is the lateral shear displacement of the bottom divided by the length of deformed nanocrystal (i.e., the maximum migration displacement

of LAGB). In the snapshot at 62 s (Figure 1h), the LAGB, dislocations, and nanotwins were all annihilated. The width of the pre-existing twin was reduced by three atomic planes at 62 s compared to the as-fabricated Au nanocrystal, which is because part of the dislocations sliding on the pre-existing TB reach the free surface during the shear load and release as the surface step, as shown in the Supplementary Figure 5. The shear deformation induced formation of LAGB and nanotwins seem to be fully reversible with negligible damage accumulation upon reversed shear load.

3.2. The influence of free surface

To understand the insight of nanotwin nucleation observed in experiments, we used the molecular dynamics (MD) method to simulate the deformation of Au single crystals under reciprocating shear load. Two nanocrystals with the same crystal orientation as that used in our experiment, but without pre-existing twin and slightly different surface slopes, were considered. The detailed model setups are illustrated in Supplementary Figure 2. The initial structure of the dynamic region in the model 1 is displayed in Figure 2a. The evolution of partial dislocations and nanotwins is shown in Figure 2b-e (Supplementary Movie 2). It can be seen in Figure 2b and c that partial dislocations and nanotwins nucleated from the free surface, and aligned to form boundaries with lattice rotation, as indicated by the blue arrows. With the increasing shear deformation, the boundaries migrated upward (Figure 2c). Upon reversal of shear load (Figure 2d, e), the boundaries migrated backward and were fully annihilated with negligible damage accumulation. Figure 2f shows the spatial distribution of lattice misorientation at the deformation stage shown in Figure 2c, demonstrating lattice rotation of the formed boundaries in the nanocrystal under shear load. The enlargement in Figure 2g shows the upper boundary with misorientation angle of 8° is near the (111) TB at the end of rightward shear load. While the enlargement in Figure 2h shows the lower boundary is a TB with interactive nanotwins.

Our experimental and MD simulation results corroboratively show that 1) partial dislocations and nanotwins nucleate on free surfaces; 2) LAGB forms at the head of aligned nanotwins; and 3) The nanotwin-assisted LAGB formation is reversible under reciprocating shear load. Twins in fcc metals usually propagate with a high velocity once nucleated[26]. However, nanotwin alignment here causes a lattice rotation as shown in Figure 1 and 2, hence, a curved slip plane. Meanwhile,

the lattice rotation angle increases with the increase of the density of aligned nanotwins. The stress needed to overcome the Peierls barrier (lattice resistance to dislocation motion) on the curved slip planes increases[27]. Furthermore, the Peierls stress increases when twinning partials propagate from the free surface to the inner region[28]. Therefore, the velocity of nanotwins decreases with the increase of nanotwin density when it propagates from free surface. As consequences, the nanotwins align to form LAGB, and the migration velocity of LAGB decreases as shown in Figure 1i.

Obvious differences in partial dislocation and nanotwin response can also be observed between experimental and MD simulation result. For example, the MD results (Supplementary Movie 2) show that two slip systems are activated. On free surfaces, the slip system on (111) was first activated and forms nanotwins (Supplementary Figure 6a), then the slip system on (-1-11) was activated (Supplementary Figure 6b). Along with increasing shear stress, the (-1-11) slip system became the dominated one with more partial dislocations and nanotwins (Figure 2c). There are totally two LAGBs and one TB formed during the shear deformation since two slip systems are both activated in MD simulation (Figure 2b-d). In experiments, however, only one slip system on (-1-11) is activated, and one LAGB forms. From the applied shear stress in MD simulations, the largest resolved shear stress is on (111) plane. It is expected that the slip system on (111) be first activated like the MD results. The reasons why the slip system on (111) is not activated in the experimental sample could be 1) the pre-existing twin reduces the resolved shear stress on (111) and increases the resolved shear stress on (-1-11), and 2) the morphology of free surfaces such as roughness and surface angles respect to the shear direction may affect the resolved shear stresses on slip planes. For the former one, we indeed observed the (111) slip system was first activated in the nanocrystal with similar orientations but without pre-existing twin during shear load (as shown in Supplementary Figure 7 and Supplementary Movie 3). For the latter one, we designed a crystal denoted as model 2 to study the influence of free surface morphology on the nanotwin formation. The results are shown in Figure 3 and the Supplementary Movie 4. Coincidently, the model 2 shows similar deformation process with the nucleation of partial dislocations, nanotwins and boundaries. However, the slight change of surface steepness dramatically reduces the nucleation of nanotwins on (111) plane and increase the nucleation of nanotwins on (-1-11) on free surface, as shown in Figure 3b-d. Besides, the misorientation angle of the upper boundary increased to 11°

in model 2 (Figure 3g). The results indicate that a slight change in crystal surface morphology affects the preferred nucleation of nanotwins. It confirms the steeper free surface could be one reason of the suppressed activity of (111) slip system in our experimental observation. The other differences we noticed is the propagation of partial dislocation nucleated at the fixed boundary and free surface between MD simulation and experimental result. This phenomenon due to the pre-existing twin in the experiment makes the strain at the fixed boundary mostly concentrated inside the twin (as the high-density defects inside the twin form the end boundary in Figure 2b-f). The other reason is that the thickness of nanocrystal near free surface region (within several atom layers) in experimental may have steepness to reach zero, which is not as the uniformity in MD simulation. It will make the energy barrier for partial dislocation nucleation at free surface decrease, resulting the partial dislocation nucleated largely at the free surface (as in experimental results). Beside these differences in details, the MD simulation result of model 1 and 2 apparently leads to the same mechanism of nanotwin assisted LAGB formation under the shear deformation.

3.3. Atomistic mechanism of the reversible LAGB formation

To further unveil the atomic level deformation mechanism on the nanotwin assisted reversible LAGB formation, we analyzed the details of MD simulation results and the HRTEM snapshots. The dislocation dipole with two partial dislocations sliding along the TB has been observed in the MD simulation as shown in Figure 4. The snapshots in Figure 4a-c show the distance between the two dislocations decreases with the increasing shear deformation. Figure 4d clearly indicates the dipole at the TB generates a full dislocation with excess (111) plane and burgers vector 1/2[101]. The experimental HRTEM snapshots at the initial shear deformation clearly show that the dislocations associated with the LAGB all have a feature of excess (111) plane (Figure 1b-d and 5a). Considering the 1/3<111> type Frank partial dislocation is sessile, the dislocation is speculated to be the 1/2<101> type full dislocations. The TB acting as a slip plane for the partial dislocations has been reported to be a soft mode for deformation[29, 30]. The dislocation core observed in the experiment appears to be compact, with negligible dissociation as reflected by the corresponding shear strain distribution obtained by geometrical phase analysis (GPA) in Figure 5a and 5b[31]. This phenomenon could be explained by the slightly different Schmid factor of different dislocation types. According to the nanocrystal orientation in the experiment (Figure 5e), the angle between shear direction and δA is smaller than that of Bδ, implying the Schmid factor

(Schmid factor = cosφcosλ) for the trailing partial dislocation (δA) is bigger than for the leading partial dislocation (Bδ). Therefore, a nucleated leading partial dislocation is swiftly followed by a nucleated trailing partial dislocation to slip upward, leading to a generation of the full dislocation (BA) with compact core. However, during the reversal shear deformation, nucleation and propagation of additional partial dislocations is required to accomplish the detwinning process, consequently resulting in the complex dislocation reaction and strain distribution near the LAGB (Figure 5c and d).

Combining our experimental and simulation results, we deduce the deformation sequence of the reversible LAGB formation as follow. Upon shearing, nanotwins generate from free surface and grow inside with the Shockley partial dislocation (i.e. Cδ, Bδ, δA in Figure 5e) gliding. This nanotwins formation with Shockley partial dislocation nucleation and propagation had been confirmed by our simulation result(Figure 2 and 3) and also documented in Au nanocrystals below 10 nm range under tensile load[32]. At the meantime, some Shockley partial dislocations with different Burgers vectors emit from free surface, glide at the TB planes, and coalesce to generate the full dislocations (i.e., Bδ + δA → BA in Figure 5e). These full dislocations align at the tip of nanotwin to form the LAGB. Upon reversed shearing, LAGB migration associated with detwinning is accomplished. However, during the reversal shear deformation, nucleation and propagation of additional partial dislocations is required to accomplish the detwinning process, consequently resulting in the complex dislocation reaction and strain distribution near the LAGB (Figure 5c and d). Therefore, the reversible shear deformation behavior involving LAGB formation and annihilation is realized by the simultaneous nanotwin formation and dislocation glide on TB inside the Au nanocrystal, which we term as the nanotwin-mediated dislocation slip mechanism, as schematically shown in Figure 5f. During the shear deformation process, the TB provides an easy slip plane for dislocations, meanwhile the dislocations arrange parallelly to create a LAGB to accommodate the huge lattice rotation at the head of the nanotwins.

To gain a quantitative information on the shear load that is needed to initiate reversible formation of the LAGB, the shear load (estimated from applied stress on the bottom layer of atoms) and displacement at 30 ps and 48 ps (LAGB formed) are 25.6 MPa, 3 nm and 170 MPa, 4.8 nm in simulation model 1, respectively. Therefore, the required shear load to initiate the LAGB is around 25.6–170 MPa. But this critical shear load might depend on the sample geometry, size and other

factors, such as loading rate and temperature. From the results observed in the experimental sample and MD models, we conclude that the LAGB is reversible under an opposite shear load as long as the plastic deformation could be accommodated by LAGB formation without generating other severe damage such as cracks.

3.4. Shear deformation accommodated by twinning and detwinning

The crystal orientation and the pre-existing twin have been noticed to be key factors that control the deformation mechanism, which is confirmed by the deformation behavior of a nanocrystal that contained a pre-existing twin with different orientation (Figure 6 and Supplementary Movie 5). The HRTEM of as-fabricated Au nanocrystals indicate the pre-existing twin had the (111) TB planes (Figure 6a). The shear load direction was nearly parallel to the twin boundary plane (Figure 6b). We found the plastic deformation was accomplished by the narrow down and annihilation (detwinning) of the pre-existing twin under shear load (Figure 6b and c). Upon reversed shear load, we observed the re-nucleation and broadening (twinning) of deformation twin with (111) TB plane (Figure 6d-f). Comparing the nanocrystal microstructure in Figure 6a and f, we found the plastic deformation was again reversible. These result shows prefect consistency with the recent report of the TB shear deformability[33], confirming the importance of the TB orientation in determining the deformation mechanism.

4. Discussion

The shear induced GB formation and migration plays an important role in plastic deformation of metallic materials during SPD at room temperature. For the shear induced GB migration, some *in-situ* TEM works had directly observed and unraveled the mystery of the dynamic mechanism under atomic scale, for example, atomic shuffling[34], GB dislocation/disconnection[35, 36]. For the GB formation, although there is one previous report by *in-situ* TEM[37], the mechanism is not general and clearly lack of direct linkage to shear strain due to the complex localized strain distribution upon bending. The grain refinement, strongly associated with GB formation, has two well-accepted mechanisms dominated by dislocation activity[18, 38] and twinning[39, 40], respectively, which shows dependence on the intrinsic stacking fault energy (SFE) of the materials, specimen size, and the deformation conditions, such as strain, strain rate, temperature. Our *in-situ* TEM observation on the dynamic formation process of LAGB in Au nanocrystal unveils atomic

details featuring the cooperation between nanotwins and full dislocations. This nanotwin-mediated dislocation slip mechanism for LAGB formation shows excellent reversibility under reciprocating shear load, which seems different from irreversible shear localization and structural degradation that commonly happens in metallic nanomaterials with non-conservative defect activities[41]. Therefore, we deduce participation of nanotwins is critical for the reversibility of LAGB formation. Based on previous studies, twinning, as a common deformation mode, introduces coherent interfaces (i.e., TB), which in one way acts as strong barriers to hinder dislocation activities and effectively increase the strength of materials[42, 43], meanwhile in other way provides nucleation sites and slip plane for glissile dislocations, contributing to the excellent mechanical properties defeating the traditional trade-off between strength and ductility[30, 44, 45]. As demonstrated in our experimental and simulation results, the generated nanotwins with same TB plane strongly suppress the activity of the other slip system during deformation (the partial dislocation crossing the TB will be blocked, as the MD result in Supplementary Figure 8). Moreover, these TBs act as an easy slip plane for dislocations, which could assist the rearrangement of dislocations during formation of LAGB and the backward slip of dislocations during the reversed annihilation. Therefore, the deformation reversibility observed in this work is the result of synergistic action including nanotwins and full dislocations, which is different from the previously proposed mechanisms of either defects uninvolved or only associated with one specific defect type[35, 46-48]. It should be noticed that dimension of nanocrystal will affect the formation of nanotwin and full dislocations during deformation, as has been generally reported in nanocrystals[6-9, 49].

The crystal orientation, nanocrystal geometry and pre-existing twin play a very important role to perform this nanotwin-mediated dislocation slip mechanism. When the shear direction has a small angle (within 20° in our experiments) with [-1-11] direction, the slip systems with (111) plane with larger Schmidt factor should be preferred than these in (-1-11) plane, demonstrated by the factor that the shear deformation is dominated by twinning and detwinning of the nanocrystal with pre-existing (111) twin (Figure 6). But the nanotwins we observed in Figure 1 all have the (-1-11) TB plane, which may associate with the specimen geometry through two aspects. On the one hand, the geometry with steeper free surface of nanocrystal suppresses the activity of the (111) slip system, which is demonstrated by the simulation results of two models as discussed above (Figure 2 and 3). On the other hand, the pre-existing (-1-11)[112] twin restrict the (111) slip system

actuation, resulting in the preferential (-1-11) slip system. Therefore, the highly selective orientation of slip system may make a great contribution to perform the reversible shear deformation with this nanotwin-mediated dislocation slip mechanism. Furthermore, this mechanism may be broadly applicable to the LAGB formation behavior in other fcc metals, especially those with low and/or medium stacking fault energies.

5. Conclusion

The present *in-situ* TEM coupled with MD simulation yield unprecedented atomic details on the formation and annihilation of LAGB in metallic nanocrystal under reciprocating shear load. We reveal a nanotwin-mediated dislocation slip mechanism for LAGB formation, featuring the formation of full dislocation with coalescence of partial dislocation gliding on the TB. The cooperation of nanotwin and full dislocation makes the nanocrystal to accommodate large shear deformation and shows excellent reversible behavior. In addition, the mechanism is found to be related to the specific deformation conditions, including nanocrystal geometry, orientation, and pre-existing twin. Considering both the formation mechanism of GB and nanotwin are common in metals under deformation, the mechanisms should be generally applicable to other fcc metallic nanocrystals. Moreover, the stacking fault energy may be an important factor since it affects the nanotwin formation. These findings offer new insights for understanding the LAGB formation, providing guidelines for designing nanodevices with ultrahigh and recoverable shear capability for advanced applications.

Declaration of Competing Interest

The authors declare that they have no known competing financial interests or personal relationships that could have appeared to influence the work reported in this paper.

Acknowledgements

This work was supported by the Laboratory Directed Research and Development (LDRD) program at Pacific Northwest National Laboratory (PNNL) as part of the Solid Phase Processing Science Initiative (SPPI). A portion of this research was performed using facilities at the Environmental Molecular Sciences Laboratory (EMSL), a national scientific user facility sponsored by the U.S.

Department of Energy's (DOE's) Office of Biological and Environmental Research and located at PNNL. PNNL is a multiprogram national laboratory operated by Battelle for the DOE under Contract DEAC05-76RL01830.

Supplementary materials

Supplementary material associated with this article can be found, in the online version, at doi: 10.1016/j.actamat.2022.117850.

References:

[1] Y. Estrin, A. Vinogradov, Extreme grain refinement by severe plastic deformation: A wealth of challenging science, Acta Mater. 61(3) (2013) 782-817.
[2] R.Z. Valiev, R.K. Islamgaliev, I.V. Alexandrov, Bulk nanostructured materials from severe plastic deformation, Prog. Mater Sci. 45(2) (2000) 103-189.
[3] I.A. Ovid'ko, Deformation of Nanostructures, Science 295(5564) (2002) 2386-2386.
[4] H. Van Swygenhoven, Grain Boundaries and Dislocations, Science 296(5565) (2002) 66-67.
[5] J.R. Greer, D. Jang, X.W. Gu, Exploring Deformation Mechanisms in Nanostructured Materials, JOM 64(10) (2012) 1241-1252.
[6] M. Chen, E. Ma, K.J. Hemker, H. Sheng, Y. Wang, X. Cheng, Deformation Twinning in Nanocrystalline Aluminum, Science 300(5623) (2003) 1275.
[7] S.H. Oh, M. Legros, D. Kiener, P. Gruber, G. Dehm, In situ TEM straining of single crystal Au films on polyimide: Change of deformation mechanisms at the nanoscale, Acta Mater. 55(16) (2007) 5558-5571.
[8] M. Ke, S.A. Hackney, W.W. Milligan, E.C. Aifantis, Observation and measurement of grain rotation and plastic strain in nanostructured metal thin films, Nanostruct. Mater. 5(6) (1995) 689-697.
[9] J. Schiøtz, F.D. Di Tolla, K.W. Jacobsen, Softening of nanocrystalline metals at very small grain sizes, Nature 391(6667) (1998) 561-563.
[10] Z. Shan, E.A. Stach, J.M.K. Wiezorek, J.A. Knapp, D.M. Follstaedt, S.X. Mao, Grain Boundary-Mediated Plasticity in Nanocrystalline Nickel, Science 305(5684) (2004) 654-657.
[11] K. Nakashima, Z. Horita, M. Nemoto, T.G. Langdon, Influence of channel angle on the development of ultrafine grains in equal-channel angular pressing, Acta Mater. 46(5) (1998) 1589-1599.
[12] X.C. Liu, H.W. Zhang, K. Lu, Strain-Induced Ultrahard and Ultrastable Nanolaminated Structure in Nickel, Science 342(6156) (2013) 337-340.
[13] D.A. Hughes, N. Hansen, Graded nanostructures produced by sliding and exhibiting universal behavior, Phys. Rev. Lett. 87(13) (2001) 135503.
[14] Y. Gao, Z. Jin, Interactions between lattice dislocation and Lomer-type low-angle grain boundary in nickel, Computational Materials Science 138 (2017) 225-235.
[15] N. Tao, H. Zhang, J. Lu, K. Lu, Development of Nanostructures in Metallic Materials with Low Stacking Fault Energies During Surface Mechanical Attrition Treatment (SMAT), MATERIALS TRANSACTIONS 44(10) (2003) 1919-1925.
[16] F. Mompiou, D. Caillard, M. Legros, Grain boundary shear–migration coupling—I. In situ TEM straining experiments in Al polycrystals, Acta Mater. 57(7) (2009) 2198-2209.
[17] X. Chen, Z. Han, K. Lu, Wear mechanism transition dominated by subsurface recrystallization structure in Cu–Al alloys, Wear 320 (2014) 41-50.
[18] K. Wang, N.R. Tao, G. Liu, J. Lu, K. Lu, Plastic strain-induced grain refinement at the nanometer scale in copper, Acta Mater. 54(19) (2006) 5281-5291.
[19] N.R. Tao, K. Lu, Nanoscale structural refinement via deformation twinning in face-centered cubic metals, Scripta Mater. 60(12) (2009) 1039-1043.
[20] S. Plimpton, Fast parallel algorithms for short-range molecular dynamics, J. Comput. Phys. 117(1) (1995) 1-19.
[21] G. Grochola, S.P. Russo, I.K. Snook, On fitting a gold embedded atom method potential using the force matching method, The Journal of chemical physics 123(20) (2005) 204719.
[22] I. Dillamore, R. Smallman, The stacking-fault energy of FCC metals, Philos. Mag. 12(115) (1965) 191-193.
[23] A. Stukowski, Visualization and analysis of atomistic simulation data with OVITO–the Open Visualization Tool, Modell. Simul. Mater. Sci. Eng. 18(1) (2009) 015012.

[24] A. Stukowski, Structure identification methods for atomistic simulations of crystalline materials, Modell. Simul. Mater. Sci. Eng. 20(4) (2012) 045021.
[25] P.M. Larsen, S. Schmidt, J. Schiøtz, Robust structural identification via polyhedral template matching, Modell. Simul. Mater. Sci. Eng. 24(5) (2016) 055007.
[26] S. Kibey, J.B. Liu, D.D. Johnson, H. Sehitoglu, Predicting twinning stress in fcc metals: Linking twin-energy pathways to twin nucleation, Acta Mater. 55(20) (2007) 6843-6851.
[27] B. Joós, M.S. Duesbery, The Peierls Stress of Dislocations: An Analytic Formula, Phys. Rev. Lett. 78(2) (1997) 266-269.
[28] A. Dutta, M. Bhattacharya, P. Barat, P. Mukherjee, N. Gayathri, G.C. Das, Lattice Resistance to Dislocation Motion at the Nanoscale, Phys. Rev. Lett. 101(11) (2008) 115506.
[29] Q. Pan, H. Zhou, Q. Lu, H. Gao, L. Lu, History-independent cyclic response of nanotwinned metals, Nature 551(7679) (2017) 214-217.
[30] K. Lu, L. Lu, S. Suresh, Strengthening Materials by Engineering Coherent Internal Boundaries at the Nanoscale, Science 324(5925) (2009) 349-352.
[31] M.J. Hÿtch, E. Snoeck, R. Kilaas, Quantitative measurement of displacement and strain fields from HREM micrographs, Ultramicroscopy 74(3) (1998) 131-146.
[32] H. Zheng, A. Cao, C.R. Weinberger, J.Y. Huang, K. Du, J. Wang, Y. Ma, Y. Xia, S.X. Mao, Discrete plasticity in sub-10-nm-sized gold crystals, Nat. Commun. 1 (2010) 144.
[33] Q. Zhu, L. Kong, H. Lu, Q. Huang, Y. Chen, Y. Liu, W. Yang, Z. Zhang, F. Sansoz, H. Zhou, J. Wang, Revealing extreme twin-boundary shear deformability in metallic nanocrystals, Sci. Adv. 7(36) (2021) eabe4758.
[34] K.L. Merkle, L.J. Thompson, F. Phillipp, Collective effects in grain boundary migration, Phys. Rev. Lett. 88(22) (2002) 225501.
[35] Q. Zhu, Q. Huang, C. Guang, X. An, S.X. Mao, W. Yang, Z. Zhang, H. Gao, H. Zhou, J. Wang, Metallic nanocrystals with low angle grain boundary for controllable plastic reversibility, Nat. Commun. 11(1) (2020) 3100.
[36] Q. Zhu, G. Cao, J. Wang, C. Deng, J. Li, Z. Zhang, S.X. Mao, In situ atomistic observation of disconnection-mediated grain boundary migration, Nat. Commun. 10(1) (2019) 156.
[37] L. Wang, D. Kong, Y. Zhang, L. Xiao, Y. Lu, Z. Chen, Z. Zhang, J. Zou, T. Zhu, X. Han, Mechanically Driven Grain Boundary Formation in Nickel Nanowires, ACS Nano 11(12) (2017) 12500-12508.
[38] J.A. Muñoz, R.E. Bolmaro, A.M. Jorge, A. Zhilyaev, J.M. Cabrera, Prediction of Generation of High- and Low-Angle Grain Boundaries (HAGB and LAGB) During Severe Plastic Deformation, Metallurgical and Materials Transactions A 51(9) (2020) 4674-4684.
[39] Y. Cao, Y.B. Wang, X.H. An, X.Z. Liao, M. Kawasaki, S.P. Ringer, T.G. Langdon, Y.T. Zhu, Grain boundary formation by remnant dislocations from the de-twinning of thin nano-twins, Scripta Mater. 100 (2015) 98-101.
[40] Y. Zhang, J. Guo, J. Chen, C. Wu, K.S. Kormout, P. Ghosh, Z. Zhang, On the stacking fault energy related deformation mechanism of nanocrystalline Cu and Cu alloys: A first-principles and TEM study, J. Alloys Compd. 776 (2019) 807-818.
[41] L.Y. Chen, M.R. He, J. Shin, G. Richter, D.S. Gianola, Measuring surface dislocation nucleation in defect-scarce nanostructures, Nat. Mater. 14(7) (2015) 707-13.
[42] J. Wang, F. Sansoz, J. Huang, Y. Liu, S. Sun, Z. Zhang, S.X. Mao, Near-ideal theoretical strength in gold nanowires containing angstrom scale twins, Nat. Commun. 4 (2013) 1742.
[43] Z. Zhang, H. Sheng, Z. Wang, B. Gludovatz, Z. Zhang, E.P. George, Q. Yu, S.X. Mao, R.O. Ritchie, Dislocation mechanisms and 3D twin architectures generate exceptional strength-ductility-toughness combination in CrCoNi medium-entropy alloy, Nat. Commun. 8 (2017) 14390.

[44] B. Gludovatz, A. Hohenwarter, D. Catoor, E.H. Chang, E.P. George, R.O. Ritchie, A fracture-resistant high-entropy alloy for cryogenic applications, Science 345(6201) (2014) 1153-1158.
[45] D. Jang, X. Li, H. Gao, J.R. Greer, Deformation mechanisms in nanotwinned metal nanopillars, Nat Nanotechnol 7(9) (2012) 594-601.
[46] S. Lee, J. Im, Y. Yoo, E. Bitzek, D. Kiener, G. Richter, B. Kim, S.H. Oh, Reversible cyclic deformation mechanism of gold nanowires by twinning-detwinning transition evidenced from in situ TEM, Nat. Commun. 5 (2014) 3033.
[47] J. Wang, Z. Zeng, C.R. Weinberger, Z. Zhang, T. Zhu, S.X. Mao, In situ atomic-scale observation of twinning-dominated deformation in nanoscale body-centred cubic tungsten, Nat. Mater. 14(6) (2015) 594-600.
[48] L. Wang, P. Liu, P. Guan, M. Yang, J. Sun, Y. Cheng, A. Hirata, Z. Zhang, E. Ma, M. Chen, X. Han, In situ atomic-scale observation of continuous and reversible lattice deformation beyond the elastic limit, Nat. Commun. 4 (2013) 2413.
[49] Y.T. Zhu, T.G. Langdon, Influence of grain size on deformation mechanisms: An extension to nanocrystalline materials, Materials Science and Engineering: A 409(1-2) (2005) 234-242.

Figures

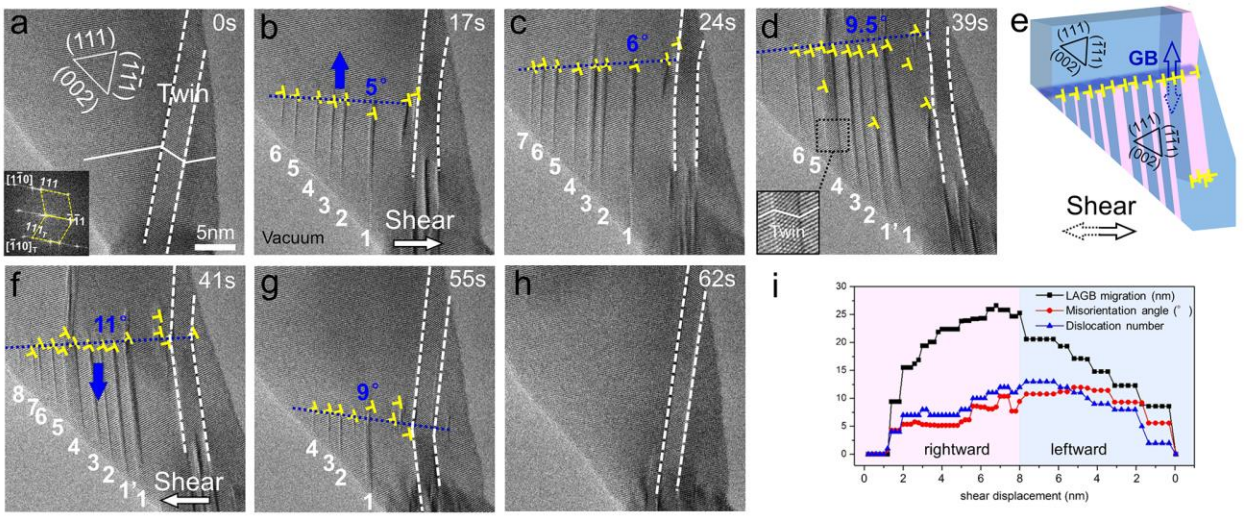

Figure 1 **Reversible LAGB formation assisted by nanotwins in an Au nanocrystal under reciprocating shear load.** (a) High resolution TEM images of an as-fabricated Au nanocrystal contained a small pre-existing twin. The white line represents the (111) plane, while dash lines indicate the twin boundaries. The triangle shows the orientation of matrix. The insert is Fast Fourier transform pattern confirming the twin relationship. (b-d) Sequential deformation snapshots show the nanotwins initiate from free surface and grow inside, which was accompanied by dislocations aligned to form LAGB under rightward shear load. The shear stress with an inclination of ~11° to the (111) plane of matrix is applied by moving the bottom side, as indicated with the white arrow. The nanotwins and dislocations are marked by the white numbers and yellow symbols, respectively. (e) The schematic shows the migration processes of LAGB consisting of a parallel dislocation array accompanied by nanotwins under shear load. The blue and pink regions represent matrix and twin, respectively. (f-h) Subsequent snapshots show the deformation recover process including LAGB backward migration along with detwinning and dislocations vanishing, as well as the fully recovered state under leftward shear load. (i) The graph of LAGB migration displacement from bottom, misorientation angle beside LAGB and dislocation number versus the shear displacement of specimen.

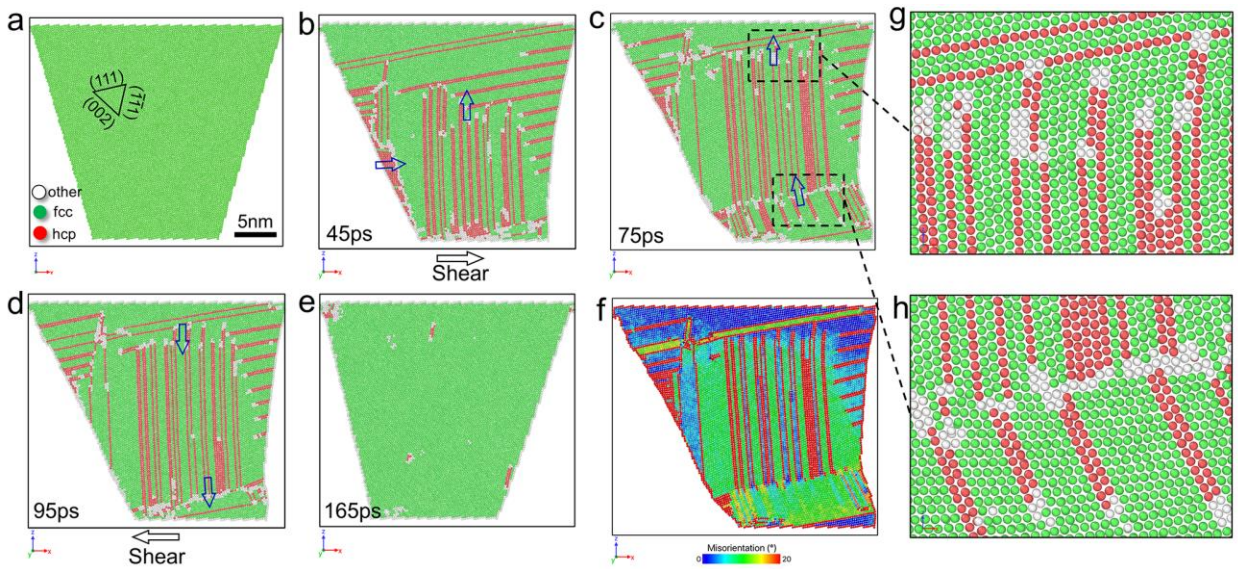

Figure 2 **Successive nucleation and annihilation of partial dislocations and nanotwins with lattice rotation under reciprocating shear load by MD simulations.** (a) Initial structure of the dynamic region of model 1 with a symmetrical geometry. (b, c) The snapshots at 45ps and 75ps under rightward shear load, respectively, demonstrating the nucleation of partial dislocations and nanotwins, accompanied by the formation of boundaries with lattice rotation. (d, e) The sequential snapshots at 95ps and 165ps under leftward shear load, demonstrating the boundaries, as well as dislocations and nanotwins migrate backward under reversed load, and fully annihilated at the end. (f) Corresponding spatial distribution of lattice misorientation of (c). (g, h) Enlargement of rectangular area marked by dash line in (c), demonstrated the atomic details of the boundaries, respectively. The blue arrows indicate the LAGB and their migration direction. The white arrows indicate the shear stress direction.

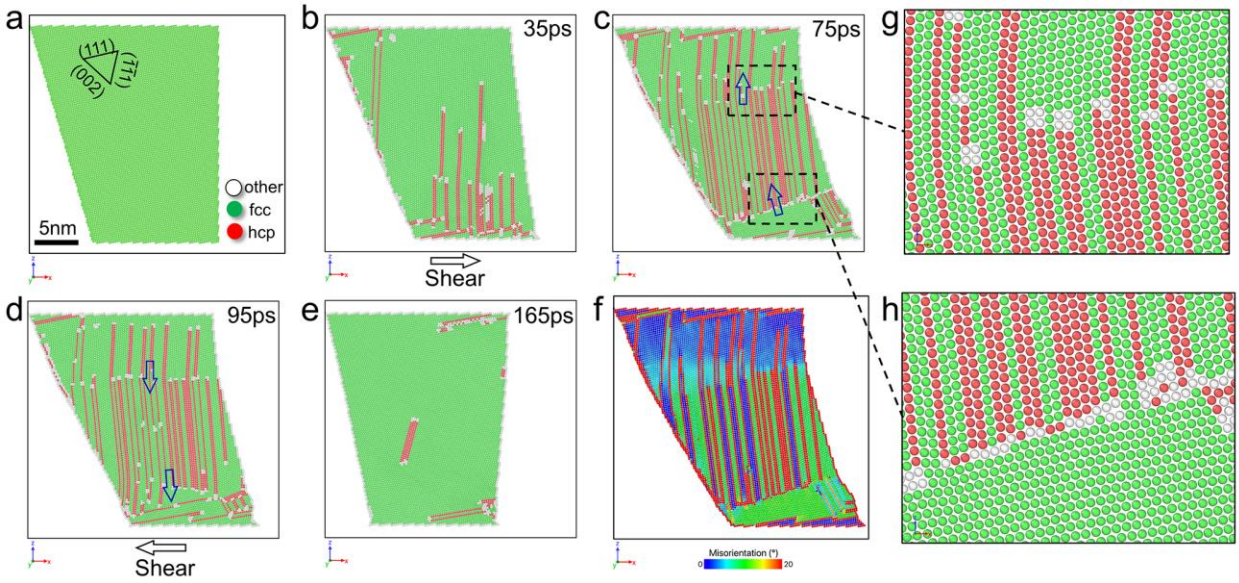

Figure 3 **The effect of surface slop on the reversible deformation explored by MD simulations.** (a) Initial structure of the dynamic region of model 2 with steeper surface than model 1. (b, c) The snapshots at 35ps and 75ps under rightward shear load, respectively, demonstrating the nucleation of nanotwins with dominant twin plane. (d, e) The sequential snapshots at 95ps and 165ps under leftward shear load, demonstrating reversible deformation under reversed load, and fully recovery at the end. (f) Corresponding spatial distribution of lattice misorientation of (c). (g, h) Enlargement of rectangular area marked by dash line in (c), demonstrated the atomic details of the boundaries, respectively. The blue arrows indicate the LAGB and their migration direction. The white arrows indicate the shear stress direction.

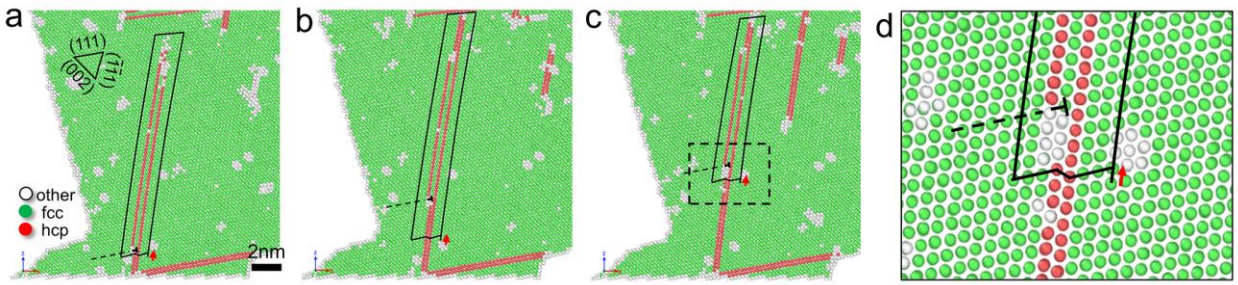

Figure 4 **MD simulation of dislocation activities.** (a-c) Dislocation dipole sliding along twin boundary. (d) Enlargement of rectangular area marked by dash line in (c), demonstrated the dislocation dipole together generates a full dislocation with one excess (111) plane.

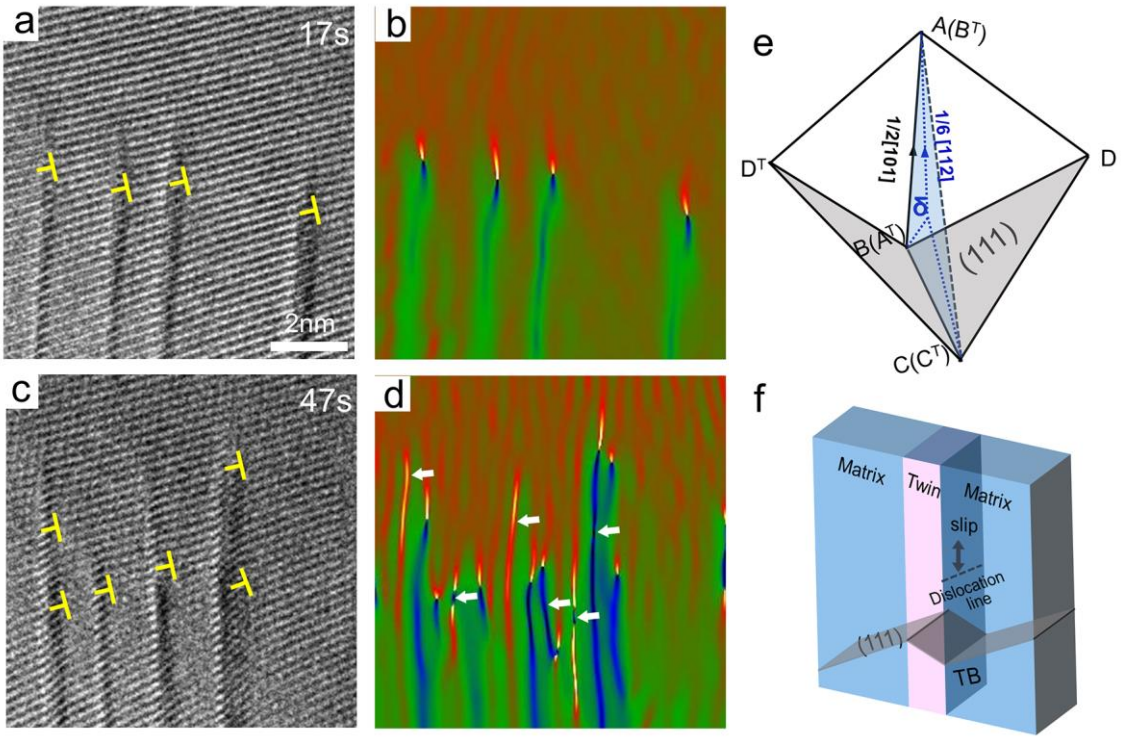

Figure 5 **Dislocations coalescence and dissociation under initial and reversed shear load.** (a, c) High resolution TEM snapshot of nanotwins with dislocations at the initial and reversed shear deformation process, respectively. (b, d) Corresponding shear strain (ε_{yx}) distribution of (a, c) obtained by geometrical phase analysis (GPA), demonstrating the dissociation of dislocation with SF formation in the recovered deformation process, as marked by the white arrows. (e) Double Thompson tetrahedron shows the slip systems and possible dislocation reaction in the nanotwin boundary plane (left: twin, right: matrix). (f) The schematic shows the nanotwin boundary acts as an easy slip plane for dislocation gliding, which assists the LAGB formation and migration.

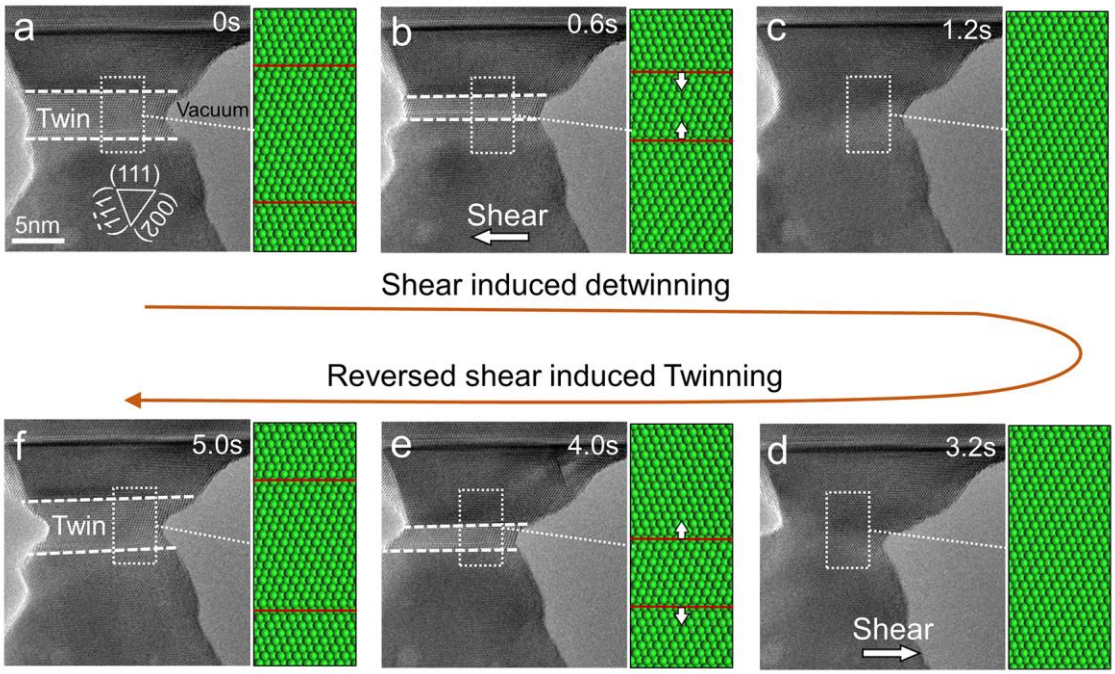

Figure 6. **The detwinning and twinning behavior in a Au nanocrystal under reciprocating shear.** (a) High resolution TEM images of an as-fabricated Au nanocrystal contained a small pre-existing twin with (111) twin planes. The white dash lines indicate the twin boundaries. The left insert shows the atomic structure in the rectangle. (b-c) Subsequent snapshots show the twin narrow down and annihilate (detwinning) under the leftward shear load. (d-f) Subsequent snapshots show the twin reappears and broadens (twinning) under the rightward shear load.